Detecting Elementary Arm Movements by Tracking Upper Limb Joint Angles with MARG Sensors

Evangelos B. Mazomenos, *Member, IEEE*, Dwaipayan Biswas, Andy Cranny, Amal Rajan, Koushik Maharatna, *Member, IEEE*, Josy Achner, Jasmin Klemke, Michael Jöbges, Steffen Ortmann and Peter Langendörfer

***Abstract*—This paper reports an algorithm for the detection of three elementary upper limb movements i.e. reach and retrieve, bend the arm at the elbow and rotation of the arm about the long axis. We employ two MARG sensors, attached at the elbow and wrist, from which the kinematic properties (joint angles, position) of the upper arm and forearm are calculated through data fusion using a quaternion-based gradient-descent method and a 2-link model of the upper limb. By studying the kinematic patterns of the three movements on a small dataset, we derive discriminative features that are indicative of each movement; these are then used to formulate the proposed detection algorithm. Our novel approach of employing the joint angles and position to discriminate the three fundamental movements was evaluated in a series of experiments with 22 volunteers who participated in the study: 18 healthy subjects and 4 stroke survivors. In a controlled experiment, each volunteer was instructed to perform each movement a number of times. This was complimented by a semi-naturalistic experiment where the volunteers performed the same movements as subtasks of an activity that emulated the preparation of a cup of tea. In the stroke survivors group, the overall detection accuracy for all three movements was 93.75% and 83.00%, for the controlled and semi-naturalistic experiment respectively. The performance was higher in the healthy group where 96.85% of the tasks in the controlled experiment and 89.69% in the semi-naturalistic were detected correctly. Finally, the detection ratio remains close ($\pm 6\%$) to the average value, for different task durations further attesting to the algorithms robustness.**

***Index Terms*—MARG sensors, orientation estimation, upper limb movement, body-area networks, gradient-descent, quaternion**

I. Introduction

The prevalence of cerebrovascular diseases (e.g. stroke) as a leading cause of death in recent years, is discussed in a number of published reports [1], [2]. For those individuals who survive a stroke episode, a long period of neurorehabilitation is required in order to regain or recover some of the lost motor functions that typically accompany a stroke. In general, the first stage of rehabilitation takes place under expert supervision at a dedicated rehabilitation center which provides everyday care and the patient's condition is constantly evaluated by medical professionals. After their discharge, patients are prescribed a customized rehabilitation program and are advised to continue their rehabilitation at home. However, home rehabilitation suffers from the fact that it is difficult for therapists to monitor the progress of the patient remotely [3], [4]. This is a key point since a major requirement for medical experts is the ability to know if the patients are capable of performing specific movements as part of their rehabilitation exercises during their everyday natural activities.

The EU funded StrokeBack project, of which this work is a part, proposes to develop a body-worn sensor system that can precisely detect and recognize specific movements of the stroke-impaired arm that are of interest to the therapists, in a home-rehabilitation environment and inform therapists of the number of occurrences and the associated quality of these movements [5]. This information allows therapists to remotely evaluate the patient's rehabilitation progress in their natural environment. In this context, this work presents the design and evaluation of a detection algorithm for three fundamental movements of the upper limb, a part of the body that most often has its motor function impaired after a stroke episode. The three movements we target to detect and recognize are; reach and retrieve an object, lift an object to mouth (e.g. drink or eat) and rotation of the forearm (e.g. pouring action or turning a key). These three types of movements are present in unison or in combination in the majority of everyday tasks and were chosen under guidance from physiotherapists participating in the StrokeBack project. Their suitability as indicators of rehabilitation progress is further demonstrated by the fact that these activities are performed in the Wolf Motor Function test, an established procedure used by therapists to evaluate the level of motor function impairment in stroke survivors [6], [7].

From a kinematic perspective, the shoulder and elbow joints of the upper limb cooperate in order for the three movements to be executed. Hence, the approach we took in the formulation of our detection algorithm was to initially calculate the kinematics of the upper limb in terms of the joint angles and position of the upper arm and forearm. Accordingly, we studied the kinematic patterns of the three movements in order to derive discriminative features that allow

This work was supported by the European Union under the Seventh Framework Programme (EU-FP7), grant agreement #288692, under the project name "StrokeBack: Telemedicine System Empowering Stroke Patients to Fight Back"

E.B. Mazomenos, D. Biswas, A. Cranny, A. Rajan and K. Maharatna are with the School of Electronics and Computer Science, University of Southampton, Southampton, SO17 1BJ, U.K. (e-mail: {ebm, db9g10, awc, ar9g12, km3}@ecs.soton.ac.uk), E.B Mazomenos is also with the Centre for Medical Image Computing, UCL, London, WC1E 6BT, U.K. (email: e.mazomenos@ucl.ac.uk)

J. Achner, J. Klemke and M. Jöbges are with Brandenburg Klinik, Berlin-Brandenburg, 16321 Bernau-Waldsiedlung, Germany (e-mail: {josy.achner, ergo_n1, joebges}@brandenburgklinik.de)

S. Ortmann and P. Langendörfer are with IHP, Leibniz-Institute for Innovative Microelectronics, Im Technologiepark 25, 15236 Frankfurt (Oder), Germany (e-mail: {ortmann, langendoerfer}@ihp-microelectronics.com)

us to effectively detect them during typical everyday activities. We chose to employ Magnetic, Angular Rate (gyroscope) and Gravity (accelerometer) (MARG) sensor modules, positioned proximal to the elbow and the wrist, to derive and track the kinematic properties (angles, position) of the upper limb. Due to their small size and compactness, MARG sensors can be attached to the upper limb without hindering its movement and after appropriate data fusion and processing, can provide a good estimation of the upper limb kinematics without the need for clear line of sight; which is not the case in the more accurate, though considerably more expensive, marker-based optical or camera sensor systems. Our analysis revealed that discrimination among the three movements is possible by investigating the pattern of the shoulder and elbow flexion/extension angles and the value of the vertical coordinate (z-coordinate) of the wrist position.

The use of MARG or inertia sensors for calculating the orientation and position of the upper limb is well researched, with a plethora of techniques reported in the literature. However the work presented here is considered an extension of previous work, since it is among the first to further utilize the kinematic information for a specific purpose; in our case, to detect the three particular, though fundamental upper limb movements, known to be used as a measure for evaluating the upper extremity motor ability. Specifically, we employ MARG sensors for the purpose of tracking the orientation and position of the arm segments and to use this information to correctly detect the three arm movements. In addition, our work differs from traditional human activity recognition approaches, in that we focus on detecting the occurrence of specific tasks during natural everyday activities, instead of attempting to classify gross human activities (e.g. walking, sitting, standing) [8]–[11]. Finally, the proposed detection method, based on identifying characteristic kinematic properties of the three movements, distinguishes itself from the vast majority of activity recognition works that employ complex machine learning techniques to achieve classification. Since this work intends to be integrated in a home-based monitoring system, where body-worn battery powered sensors are used, conventional approaches for detection and recognition based on machine learning and pattern recognition methods may not be suitable, due to their significant computational complexity that renders them inappropriate for resource constrained body-worn devices. By comparison, this work employs a computationally efficient orientation algorithm, that requires 248 scalar arithmetic operations per update for the gradient-descent optimization [12], and a basic 2-link model to obtain the upper limb kinematics, complimented with a simple set of rules derived from the kinematic analysis, to detect and recognize the three movements of interest.

Although computationally inexpensive pattern recognition methods are available (e.g. Linear Discriminant Analysis (LDA)), our preliminary investigation demonstrated that a high volume of training data is required to capture the variability in the movement of different individuals in order to effectively train such classifiers. Particularly for LDA, our investigation with various features from accelerometer and gyroscope sensor data, showed that consistent results for all three movements and various individuals, with impaired and unimpaired motor abilities, is difficult to achieve [13]. Contrary to classical machine learning approaches, in this work a rule-based detection algorithm was designed to discriminate the three movements, by analyzing the kinematic patterns of the three tasks on a dataset (analysis dataset) collected from a small number of participants with unimpaired motor function. Considering that the derived set of rules is based on functional kinematic characteristics (patterns of angles, position of joints) of the upper limb during the execution of these particular tasks, we hypothesized that similar discriminating patterns, albeit with some variation, will appear when these tasks are executed by any individual, even if their motor function is impaired by a medical condition. Therefore the kinematic analysis and the formulation of the discriminating rules was performed on data obtained exclusively from unimpaired participants. The key novelty of the work presented here is the use of characteristic kinematic patterns, which are consistent and can be effectively applied for the detection of the three movements.

To validate our hypothesis we applied the detection algorithm on a different dataset (evaluation dataset) comprising both healthy volunteers and stroke survivors, performing the three tasks in two distinct type of experiments (controlled and semi-naturalistic). Our experimental investigation aims at establishing the robustness against variations, due to inter-person variability and motor function impairment, of the derived set of rules (from the controlled experiment) and revealing the extent to which the proposed algorithm can be applied for the detection of the three movements when performed as subtasks of a typical activity (from the semi-naturalistic experiment).

The remainder of this paper is structured as follows. In Section II we briefly summarize the relevant literature, while Section III details the derivation of the upper limb kinematics. The formulation of the proposed recognition algorithm is discussed in Section IV, with the experimental evaluation, performance assessment and discussion following in Section V. Conclusions are drawn in Section VI.

II. Background

Estimation of the upper limb orientation and position is achieved through fusion and processing of heterogeneous sensor data obtained from MARG or inertia sensor modules properly attached to the upper limb. With the aid of a kinematic model, the position of the individual body segments (upper arm, forearm) can be determined in 3D space. A theoretical study on the required number of modules that need to be attached for a full orientation analysis of the upper limb is provided in [14]. The majority of the proposed solutions in the literature are based on the established Kalman Filter and its derivatives as the sensor fusion algorithm for estimating orientation [15]–[19], though more computationally efficient alternatives based on complementary filters and gradient-descent methods have also been reported [12], [20].

In recent years, the recognition and classification of basic body postures and daily activities using data from wearable MARG or inertia sensors has been an active research topic. Some of the application scenarios considered are those of rehabilitation, chronic care management and elderly population

monitoring [8]–[10], [21]–[24]. Typically, the data obtained are used to derive a set of features which are then used as inputs in various machine learning and/or pattern recognition systems for classification. For example, decision trees and neural networks were employed in [25], [26], support vector machines (SVM) in [27], [28], hidden Markov-models (HMM) in [29] and template matching in [11]. Although these approaches demonstrated very good performance, their objective was to classify gross human activities (e.g. lying, sitting, walking, running, climbing stairs etc). By comparison, the work that is reported here has a significantly different objective: to detect and classify specific arm movements, of which the longitudinal variation in their number of occurrences could potentially serve as an indicator of rehabilitation progress.

III. Deriving the upper limb kinematics

Movements of the human upper limb occur in one of the three cardinal planes of the body (sagittal, frontal and transverse) and around three corresponding axes (mediolateral, anteroposterior and longitudinal). The three planes are mutually orthogonal and the three axes are orthogonal both to each other and their corresponding planes. To represent the upper-limb we employ a 2-link limb model, depicted in Fig. 1. The upper arm and forearm are modeled through link 1-2 and 2-3 respectively. The shoulder joint is represented by joint 1, which is fixed at the origin of the global coordinate frame, while the elbow is modeled by joint 2, which connects the two links. To track the upper limb during movement, two MARG sensors are placed proximal to the wrist and elbow near points 2 and 3, as shown in Fig. 2. By continuously calculating the orientation of the MARG sensors, we can determine the orientation and position of the upper limb joints in space during dynamic movements, with respect to the 2-link model. This allows us to estimate the 5 degrees of freedom (DoF) of the upper limb, 3 DoF at the shoulder and 2 DoF at the elbow, that correspond to the angles of shoulder flexion/extension, shoulder adduction/abduction, upper arm medial/lateral rotation, elbow flexion/extension and forearm pronation/supination. This information is then fed into a detection algorithm to discriminate between the three arm movements. Based on this model, the orientation and position of the two limb segments can be defined against a static global coordinate frame, with its origin placed on the shoulder joint. Additionally, a local coordinate frame (body coordinate frame), which rotates dynamically following the rotations of the link, is applied in each link of our model, with its origin being in the shoulder and the elbow joints for the upper arm and forearm respectively. These body coordinate frames are used to obtain the initial orientation of each limb, using the MARG sensor data, which are provided in terms of their respective coordinate frames, and then mapped with respect to the global coordinate frame to enable the calculation of the joint angles and the links' position. For simplicity we chose to consider the local coordinate frame (body frame) of the upper arm and forearm to align with the coordinate frame of the sensor. Therefore, the orientation output represents not only the orientation of the MARG sensor but also the orientation of the body segment upon which the sensor platform is attached.

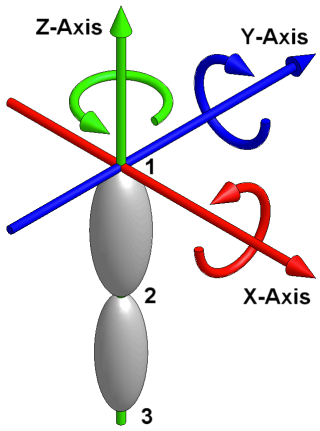

Fig. 1. The 2-link limb model we utilize to represent the upper limb and the definition of the global coordinate system.

Among the different mathematical representations of the 3-D orientation of a rigid body we elect to use quaternions in our work to express the orientations of the upper limb body segments. Quaternions demonstrate significant advantages over both Euler angles and rotation matrices in representing the orientation of a rigid body. The singularities issue (that affects Euler angles and rotation matrices) is not present in quaternion representation, which is also known to provide more robust results during orientation calculations.

The initial orientation (expressed in the body coordinate frame) of the upper arm and forearm is obtained from estimating the 3-D orientation of the MARG sensor attached to it. This is achieved by fusing the data from the accelerometer, gyroscope and magnetic field sensors and then employing a quaternion gradient-descent orientation algorithm, originally reported in [12], to calculate the MARG sensor 3-D orientation during the movements of the arm. In this algorithm, the gyroscope output (ω) can be used to derive the orientation rate of change ($\dot{\mathbf{q}}_1$) of the static reference frame (global) against a dynamic one (sensor). This is expressed, in quaternion representation as:

$$\omega_{\mathbf{q}} = [0\ \omega_x\ \omega_y\ \omega_z] \tag{1}$$

$$\dot{\mathbf{q}}_1 = \frac{1}{2}\hat{\mathbf{q}}_1 \otimes \omega_{\mathbf{q}} \tag{2}$$

Here, the operator $\otimes$ corresponds to quaternion multiplication. An estimation of the orientation ($\hat{\mathbf{q}}_1$) of the global frame relative to the sensor frame can then be calculated by integrating the quaternion derivative $\dot{\mathbf{q}}_1$ over time, given an initial condition and the sampling frequency being known.

In addition, by assuming that the other two types of sensor (the accelerometer and magnetometer) are continuously subjected to the constant fields of gravity (g) and magnetic north (m_n) with respect to the sensor coordinate frame, and given that the orientation of these two fields in the global coordinate frame is known and constant, the measurement of these fields in the sensor frame enables the orientation of that frame against the global frame to be estimated. This is formulated as an optimization problem that attempts to find a quaternion ($\hat{\mathbf{q}}_2$) solution that corresponds to an orientation

that aligns the constant field of the global frame ($\mathbf{f_g}$) to the measured one ($\mathbf{f_s}$) [12].

$$\min_{\hat{\mathbf{q}}_2} f(\hat{\mathbf{q}}_2, \mathbf{f_g}, \mathbf{f_s}) \tag{3}$$

$$f(\hat{\mathbf{q}}_2, \mathbf{f_g}, \mathbf{f_s}) = \hat{\mathbf{q}}_2^* \otimes \mathbf{f_g} \otimes \hat{\mathbf{q}}_2 - \mathbf{f_s} \tag{4}$$

Here, $\hat{\mathbf{q}}_2^*$ denotes the conjugate quaternion. The gradient-descent optimization algorithm is employed to produce a quaternion solution based again on an initial condition and of course a step size. Each field individually can not provide a unique quaternion solution, but a range of orientation solutions. The two fields are thus combined in order to produce a single quaternion solution $\hat{\mathbf{q}}_2$ that describes the sensor orientation against the global reference frame.

The two independent approximations of the orientation $\hat{\mathbf{q}}_1$ and $\hat{\mathbf{q}}_2$ suffer from intrinsic limitations related to the sensor systems. For $\hat{\mathbf{q}}_1$, the accumulation of gyroscope errors will result in a distorted estimation, while $\hat{\mathbf{q}}_2$ will suffer from the addition of linear accelerations and magnetic interference. This necessitates the fusion of the two estimates in a weighted manner, so that each one mitigates the limitations of the other. Ultimately, following a number of simplifications related to the convergence step of the gradient-descent method, the final orientation estimation is achieved from the integration of the rate of change of orientation (measured by gyroscopes), after the magnitude of the gyroscope error, denoted as β, is subtracted, alongside a direction specified by the accelerometer and magnetometer measurements (see Eq. 6). Furthermore, a mechanism for compensating magnetic distortions (soft iron errors) is in place, to limit the errors caused from them to only affect the angle of rotation around the global z-axis (yaw).

$$\mathbf{q}_t = \hat{\mathbf{q}}_{t-1} + \dot{\mathbf{q}} \cdot \Delta t \tag{5}$$

$$\dot{\mathbf{q}} = \dot{\mathbf{q}}_\mathbf{1} - \beta \frac{\nabla f}{\|\nabla f\|} \tag{6}$$

The derived quaternion orientation for each MARG sensor is expressed with respect to the sensor's coordinate frame. Obviously the orientation obtained can also be expressed with Euler angles or rotation matrices using the appropriate transformations.

To locate the position of the upper arm and forearm during movements, we define two position vectors ($\mathbf{v}_u$, $\mathbf{v}_f$) in our model structure, as illustrated in Fig. 2, which also depicts the placement of the sensors. The two position vectors are defined with respect to the body frame of the upper arm and forearm respectively. The x-axis of these frames is aligned with the direction of the upper arm and forearm when the arm is lying prone against the side of the body. Thus, the position vector of the forearm would be ${}^b\mathbf{v}_f = [-l_f \ 0 \ 0]$ while the one for the upper arm would be ${}^b\mathbf{v}_u = [-l_u \ 0 \ 0]$, where l_f and l_u are the lengths of the forearm and upper arm respectively. The location of the upper arm and forearm in the global coordinate frame is determined by transforming the position vectors from the body coordinate frame to the global one using the orientation quaternions obtained from each sensor ($\mathbf{q}_w$,$\mathbf{q}_e$). This is achieved from the following set of equations where the superscripts g and b denote the global and body reference frames respectively:

$${}^g\mathbf{v}_u = \mathbf{q}_w \otimes {}^b\mathbf{v}_u \otimes \mathbf{q}_w^* \tag{7}$$

$${}^g\mathbf{v}_f = \mathbf{q}_w \otimes {}^b\mathbf{v}_f \otimes \mathbf{q}_w^* + {}^g\mathbf{v}_u \tag{8}$$

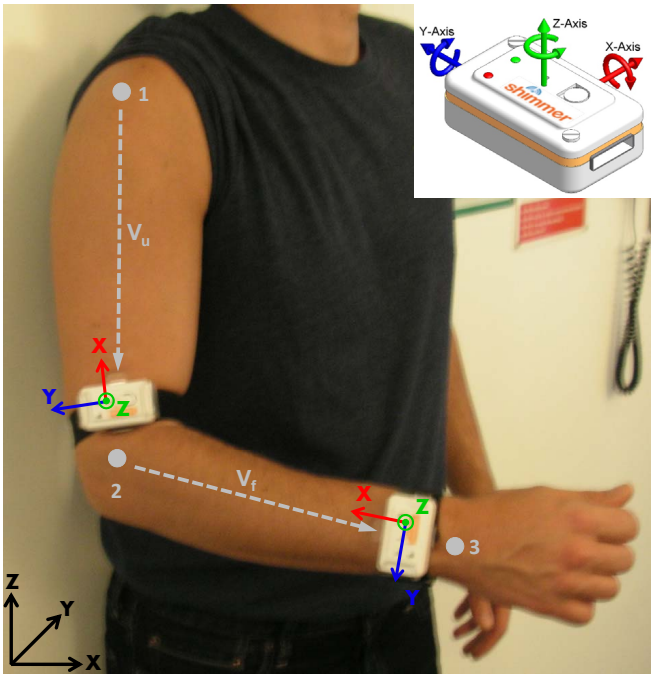

Fig. 2. The employed set-up for the kinematic analysis adapted to the two-link upper limb model of Fig. 1. The two MARG sensors (Shimmer 2r) are placed near the elbow (point 2) and wrist (point 3) with their corresponding sensor frame (upper right corner) and the global coordinate system (lower left corner) shown. The two position vectors $\mathbf{v}_u$, $\mathbf{v}_f$ are also indicated.

The 5 joint angles are calculated using the two position vectors (${}^g\mathbf{v}_u$, ${}^g\mathbf{v}_f$) as described in the following sections.

A. *Shoulder angles*

The shoulder flexion/extension (s_fe) and abduction/adduction (s_aa) angles are calculated from the upper arm position vector, while the shoulder medial/lateral (s_ml) rotation angle is calculated from the forearm position vector as follows.

$$s\_fe = 90^\circ + atan2({}^g\mathbf{v}_u(z), {}^g\mathbf{v}_u(x)) \tag{9}$$

$$s\_aa = 90^\circ + atan2({}^g\mathbf{v}_u(z), {}^g\mathbf{v}_u(y)) \tag{10}$$

$$s\_ml = \begin{cases} atan2({}^g\mathbf{v}_f(y), {}^g\mathbf{v}_f(x)), s\_fe < 90^\circ \ \& \ s\_aa < 90^\circ \\ atan2({}^g\mathbf{v}_f(z), {}^g\mathbf{v}_f(y)), s\_fe > 90^\circ \ || \ s\_aa > 90^\circ \end{cases} \tag{11}$$

where $atan2$ is the four quadrant inverse tangent function. The value of 90° is added to bring the s_fe and s_aa angles to the standard range of $[-90^\circ, +180^\circ]$. The range of s_ml is $[-90^\circ, +90^\circ]$

B. Elbow angles

The elbow flexion/extension (e_fe) angle is calculated as the angle between the two position vectors, while the elbow pronation/supination angle (e_ps) is calculated as the roll angle (ϕ_w), the angle of rotation around the global x-axis, of the MARG sensor located at the wrist. This is calculated from $\mathbf{q}_w = [q_{w1}\ q_{w2}\ q_{w3}\ q_{w4}]$. Thus,

$$e\_fe = atan2(\|{}^g\mathbf{v}_f \times {}^g\ \mathbf{v}_u\|, {}^g\ \mathbf{v}_f \cdot {}^g\ \mathbf{v}_u) \quad (12)$$

$$e\_ps = \phi_w = atan2(2q_{w3}\cdot q_{w4} + 2q_{w1}\cdot q_{w2}, 2q_{w1}^2 + 2q_{w4}^2 - 1) \quad (13)$$

The range of e_fe is $[0°, +180°]$ and that for e_ps is $[-90°, +90°]$. The calculations listed in Eq.10-Eq.13 refer to the joint angles for the right upper limb. The calculation of s_aa, s_ml and e_ps requires minor adjustments to be made, such as change of sign for some of the position vector coordinates, when the left upper limb is considered.

IV. Data collection and kinematic pattern analysis

The kinematic information derived from the previous analysis was utilized in order to identify characteristic patterns and values that can be used for distinguishing among the three movements. This investigation was performed on a set of 28 repetitions for each of the three tasks, performed by two healthy volunteers in a controlled environment. The dataset obtained (analysis dataset) was used exclusively for the extraction of the discriminating features and for the formulation of the identification algorithm and was not included in the performance evaluation experiments (evaluation dataset), which took place both with healthy individuals (18) and stroke survivors (4), as discussed in Section V.

In the analysis dataset, the three tasks were executed sequentially in each repetition, with the subject performing them whilst sitting comfortably on a chair at a table. Initially the volunteer reached and retrieved a glass of water positioned in front of them. After the glass was retrieved the subject performed the task of arm rotation and poured the water into another, initially empty, glass. The final task performed was the task of lifting and drinking the water from the second glass before returning it to the table. The tasks were deliberately executed at a relatively slow pace in order to clearly capture their kinematic patterns. This facilitated comparison and the extraction of the discriminating features.

In our experiments we employed the Shimmer 2r 9DoF MARG sensor platform, comprised of mutually orthogonal 3-axis accelerometer, gyroscope and magnetometer. The data streams from the three sensors were used as inputs for deriving the kinematic information. The Shimmer module is based on an MSP430 microcontroller operating at 8 MHz and has an integrated RN-42 class-2 Bluetooth transceiver enabling wireless communication [30]. The operational range was set at $\pm 1.5g$ for the accelerometer and at $\pm 500°/s$ for the gyroscopes. The MARG module was programmed to sample at 50Hz which was deemed sufficiently fast for sampling elementary arm movements. The accumulated MARG data were initially filtered to remove noise, using zero-phase digital FIR filters. Accelerometer and magnetometer data were filtered with a low-pass filter with cut-off frequency at 12Hz and 10Hz respectively. Gyroscope data were filtered with a band-pass filter in the range of 0.5Hz to 25Hz. The sensors were calibrated before the beginning of the experiments, using Shimmer's proprietary software. Other Shimmer software, that permitted multiple wireless Bluetooth streams to transmit data concurrently, was used for data acquisition. During the experiments, the operator of the acquisition software manually annotated the start (on) and end (off) times of each task by adding a marker signal to the data, based on a predefined resting position, effectively segmenting each task.

The two sensors were attached to the upper arm, proximal to the elbow and proximal to the wrist, using bespoke holders with elastic straps and orientated such that their coordinate frames were closely aligned with the local coordinate frame of the upper arm and forearm. The alignment was visually inspected by instructing the subject to raise their upper arm to approximately $90°$ (shoulder height) and fully extend their elbow (palm facing downward). The conclusions we draw from the kinematic pattern analysis of each task and the description of the characteristic features that we base our identification algorithm upon, are discussed in the following paragraphs.

A. Reach and retrieve - Task A

The reach and retrieve task relates to the act of reaching in order to grasp an object and the subsequent retrieval of the object. During the reaching act, the shoulder joint is flexing while the elbow is extending concurrently. Throughout this work and in our experiments a reach and retrieve task is considered one which requires the elbow to be almost fully extended in order to reach the object. Therefore, since flexion of the shoulder results in the s_fe angle increasing while the extension of the elbow translates to the e_fe angle being decreased at the same time, one would expect that at the point when the object is reached, the s_fe value will be at a local maximum while the e_fe will demonstrate a local minimum in the same temporal frame. This kinematic pattern is illustrated in Fig. 3, produced from a representative execution of Task A.

B. Lift object to mouth - Task B

The second task we investigate relates to the act of bending the arm at the elbow. This was realized as lifting an object (e.g. glass or cup) to the mouth and drinking from it. From our observations it is revealed that the value of e_fe remains at an almost constant maximum level with minuscule variations during the act of drinking, which takes place near the midpoint of the task. Additionally, our investigation further revealed that the value of ${}^g\mathbf{v}_f$ on the z-axis (v_f^z), the vertical coordinate, becomes higher than 0m in the midpoint area of the task. This is based on the fact that the act of lifting and drinking requires the end of the forearm (wrist) to reach the height of the mouth thus having its vertical coordinate being higher ($>$ 0m) than the origin located at the shoulder. Fig.4, taken from an execution of Task B, illustrates these two characteristic features of this task.

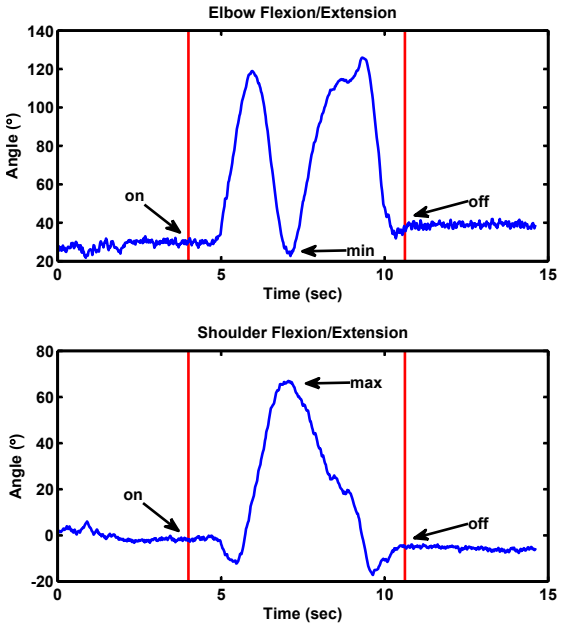

Fig. 3. Reach and retrieve s_fe and e_fe angles demonstrating the temporal proximity of the two extrema points.

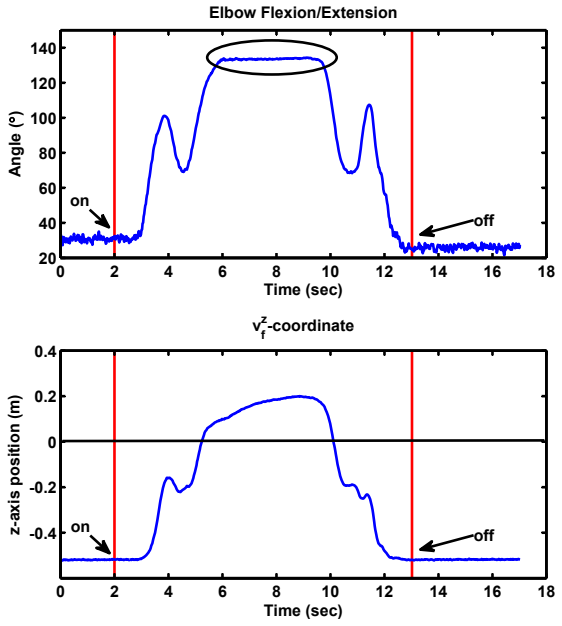

Fig. 4. The e_fe angle and v_f^z coordinate during the act of lifting an object and drinking. The area of constant e_fe is indicated by a circle and the surpassing of the 0m threshold, indicated by a solid line, is clearly visible.

C. Rotate an object - Task C

The final movement we consider is the act of rotating the arm. In our experiments, this task is realized by rotating a glass and pouring its contents to another glass. The same behavior for e_fe discussed in Task B, was also observed in Task C, where e_fe has an almost constant value with very small perturbations. Finally, through monitoring the value of ${}^g\mathbf{v}_f$ during the executions of Task C we observe that the v_f^z is always smaller than 0m. These two observations are shown in Fig.5, which shows a representative execution of Task C.

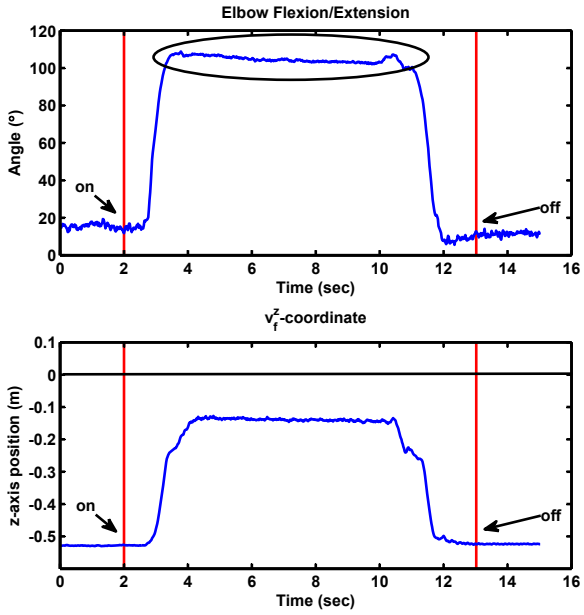

Fig. 5. The e_fe angle and v_f^z coordinate during the act of rotating the arm. The area where e_fe remains constant is indicated by a circle and the 0m threshold, is never surpassed.

D. Detection and discrimination method

The aforementioned set of observations was deduced exclusively from the analysis dataset and even though only two subjects participated in these experiments, we hypothesized that the kinematic patterns we observed will also be present during the execution of these tasks by any individual, although a certain amount of inter-person variability is expected. This stems from the fact that these kinematic patterns and the subsequent set of detection rules that we formulated, are based on the motor function of the upper limb, which is expected to have similar, more or less, characteristics even in situations where it is impaired due to a neuro-degenerative pathology. For example, the pattern associated with the act of reaching, in which the s_fe angle will increase while almost simultaneously the e_fe angle will decrease and the extrema points will appear during full extension, is due to the inherent way this task is performed. Subsequently, our strategy was to employ the analysis dataset for deriving the set of rules for discriminating the three tasks and then evaluate its robustness through experimentation, as presented in Section V, with a diverse population which included both a healthy group and stroke survivors (evaluation dataset). To summarize our findings, the kinematic analysis of the three movements has shown that discriminating among the three tasks is possible by investigating the value and pattern of three kinematic features, namely: the values of the s_fe and e_fe angles and the value of v_f^z. The specific characteristics of the kinematic features that we use to discriminate the three movements are summarized as:

- Task A: The e_fe pattern displays a steep slope and significant variations at midpoint. In addition the e_fe and s_fe angles will have extrema points (min for e_fe, max for s_fe) that are nearly coincident in time.

- Task B: The e_fe pattern remains almost constant at the midpoint. The v_f^z value will be $>$ 0m at midpoint.
- Task C: The e_fe pattern remains almost constant at the midpoint. The v_f^z value will be $<$ 0m at midpoint.

Hence, Task A can be distinguished from the other two tasks by examining the pattern of e_fe. Secondly, after eliminating Task A, a distinction between Task B and Task C is possible by investigating the value of the v_f^z at midpoint against a threshold set at 0m. Based on this set of rules, a two-level detection and discrimination algorithm is proposed as follows.

We consider the three kinematic properties (e_fe, s_fe and v_f^z) and the on/off times, provided from the manual annotation, of each task as the inputs to our algorithm. Initially, the minimum value (e_{min}) of the e_fe and its temporal position (e_p) and the maximum value (s_{max}) and its temporal location (s_p) of the s_fe are extracted. The window in which we search for these values is set as [on+1s, off-1s]. We confine our search for the two extrema points to this window, to exclude kinematic data collected at the very beginning and end of the task, which we have observed can sometimes lead to erroneous detections of the extrema points. This is due to involuntary sudden movements of the arm occurring near the beginning and end times of the task. We then extract the temporal location (m_p) and value (m_v) of the midpoint of e_fe, and count the total number of times n that the angle falls below a pre-determined fraction ($\alpha \cdot m\_v$) of the midpoint value, derived experimentally, within the temporal window [m_p-0.7s, m_p+0.7s]. Parameter n allows us to determine whether or not the e_fe values around m_p are fairly constant. This is typical of the plateau-like responses exhibited in the case of Task B and Task C and which translates to n being smaller than a experimentally derived threshold $n < 5$. By comparison the value of n is expected to be rather high $n > 5$ for Task A. Hence, the value of n acts as the discriminating factor between Task A and Tasks B and C. In the case where $n > 5$, the two extrema angles (e_{min}, s_{max}) and their temporal proximity (abs(e_p - s_p)) are checked against pre-defined thresholds and if found to be $e_{min} < 40°$, $s_{max} > 50°$ and abs(e_p - s_p)$< 0.7s$ then the task is labelled as Task A. If $n < 5$, the algorithm proceeds to the second level to distinguish the task as either Task B or Task C. For this, the maximum value (m_z) of the v_f^z in the [m_p-1s, m_p+1s] window is extracted. When compared to the 0m threshold, this parameter allows us to distinguish Task B from Task C. The proposed detection and discrimination algorithm is provided as pseudocode in Fig.6.

Initialise
Consider on, off points and the timeseries of s_fe, e_fe, v_f^z
Calculate the Parameters
- Find min(e_fe) and max(e_fe) in [on+1s,off-1s]
- Find (m_p) as m_p = on+((off-on)/2) and (m_v) from e_fe
- Count n as the number of e_fe values in [m_p-0.7s, m_p+0.7s] that $< \alpha \cdot m\_v$, $\alpha = 0.88$
- Find m_z as the max(v_f^z) value in [m_p-1s, m_p+1s]
Task discrimination
if abs($e_p - s_p$)$< 0.7s$ & $e_{min} < 40°$ & $s_{max} > 50°$ & $n > 5$ **then**
  - task = A;
else if $n < 5$ **then**
  if $m_z >$ 0m **then**
    - task = B;
  else if $m_z <$ 0m **then**
    - task = C;
  end if
end if

Fig. 6. The pseudocode of the proposed algorithm.

V. Experimental Evaluation and Discussion

A. Experimental Evaluation

In order to evaluate the performance of the proposed algorithm, we conducted a series of experiments with 18 healthy volunteers at the University of Southampton and with 4 stroke survivors at Brandenburg Klinik in Bernau, Germany; the latter under supervision of clinical staff. The healthy cohort comprised staff and students from the university, age range 25-50, with representatives from both male and female populations and examples of both left and right arm dominance. The 4 stroke survivors were men and women, age range 45-73, at different stages of their post-stroke rehabilitation. The selection of the two groups reflects our approach in evaluating the detection algorithm against two populations with noticeably different qualitative characteristics with regard to their motor function abilities. Our intention was not to perform a clinical study and test a medical hypothesis. The selection criterion for the participants was that of motor function impairment. The results obtained from the healthy volunteers provide a baseline of the algorithm's performance for normative, unimpaired motion. The experiments involving stroke survivors are used to reveal the extent to which the proposed algorithm can be applied for the discrimination of the three movements in individuals with non-canonical motor function. In other words, how the detection performance is affected by physical disability.

In these experiments, the healthy subjects used their dominant arm while the stroke survivors used their stroke-affected arm. Shimmer 2r MARG sensors were attached to the forearm (proximal to the wrist) and upper arm (proximal to the elbow) of the subjects, whilst they performed a number of arm movement exercises. The correct placement of the sensors was visually verified as described in Section IV. Physiotherapists assisted the stroke survivors in placing their arm in the desired position for placement evaluation. Whenever necessary the sensor placement was corrected.

Our study comprised two distinct types of experiment. In the first type, referred to as "controlled", each subject performed the three tasks whilst seated at a table, in a similar way as in the analysis dataset with the subject having to reach, grasp and retrieve a glass of water for Task A, pour the water into another glass for Task C and drink the water and return the glass to the table for Task B. However, in the controlled experiments the tasks were not executed sequentially, Instead each task was repeated individually 5 times on a single execution run (i.e. 5 repetitions of Task A followed by 5 of Task B and then 5 of Task C). Between task repetitions the arm was briefly returned to a resting position. This was a simply a predetermined position in which the participant paused briefly and facilitated the operator of the data collection software

to manually annotate the start and end time points of each task execution. The second type of experiments, referred to as "semi-naturalistic" involved the execution of 20 tasks in a sequence that emulated the everyday activity of "preparing a cup of tea". Every one of the 20 tasks belongs to one of the three classes of interest. Out of the 20 tasks, 10 of them were Task A, 5 Task B and 5 Task C. Our intention in the semi-naturalistic experiment, was to evaluate the performance of the proposed method with a series of tasks that when grouped together constitute a standard everyday activity. Again, the subjects briefly positioned their arm in the resting position between actions. Table I lists the sequence of the 20 tasks performed during the semi-naturalistic experiment and their respective class assignment. For the stroke survivors the study

TABLE I
THE SEQUENCE OF 20 TASKS IN THE "PREPARING A CUP OF TEA" ACTIVITY

No	Action	Class
1	Fetch cup from desk	A
2	Place cup on kitchen surface	A
3	Fetch kettle	A
4	Pour out extra water from kettle	C
5	Put kettle onto charging point	A
6	Reach out for the power switch on the wall	A
7	Drink a glass of water while waiting for kettle to boil	B
8	Reach out to switch off the kettle	A
9	Pour hot water from the kettle in to cup	C
10	Fetch milk from the shelf	A
11	Pour milk into cup	C
12	Put the bottle of milk back on shelf	A
13	Fetch cup from kitchen surface	A
14	Have a sip and taste the drink	B
15	Have another sip	B
16	Unlock drawer	C
17	Retrieve biscuits from drawer	A
18	Eat a biscuit	B
19	Lock drawer	C
20	Have a drink	B

spanned 3 weeks in order to minimize interference to their regular rehabilitation program. Each week, 4 execution runs of the controlled experiment, totaling 20 repetitions per person for each task, were performed. Over the entire 3-week study, each stroke survivor completed 60 executions of each task. The semi-naturalistic experiment was executed twice in the first week and 4 times in weeks two and three. This resulted in a total of 10 executions of the experiment for each stroke survivor, involving 100 instances of Task A and 50 of Task B and Task C. In the healthy group, each subject performed 4 runs of the controlled experiment, thus 20 repetitions of each task, and 4 of the 18 volunteers performed 4 repetitions of the semi-naturalistic experiments (40 Tasks A, 20 Tasks B and 20 Tasks C). The data gathered from these experiments constitute the evaluation database which was used for evaluating the performance and robustness of the proposed detection and discrimination algorithm. It should be noted that none of the data from these experiments was used to modify the existing algorithm, which was based exclusively on the analysis dataset as described in Section IV. The evaluation database was used explicitly for performance assessment.

Table II lists the achieved performance of the controlled experiment in the stroke survivors group. High detection performance ($> 95\%$) was observed for each individual task, the only exception being a lower value of approximately 88% for Task A in the combined results. Similar level of performance ($> 95\%$) was attained for all subjects over the three tasks, apart from Subject 3 where the overall detection accuracy was 80%. These two lower scores ($< 90\%$) are both attributed to Task A being detected with a lower degree of accuracy in the second week of experiments with Subject 3. This is illustrated in Fig. 7, which depicts the week-by-week performance achieved in the controlled experiment by the stroke survivors group. From Fig. 7(a) we observe that Task A was detected with 40% (8/20 successful detections) in week 2 for Subject 3. We also notice that Task A was detected at higher levels during the other weeks, 60% (12/20 correct detections) in week 1 and 80% (16/20 correct detections) in week 3, and that the detection of Task B for Subject 3 was also at the lowest level in week 2. These two observations prompt us to conclude that some erroneous sensor placement was the reason for this performance during the second week. Furthermore, the motor functions of Subject 3 were affected by their stroke episode more than the rest of the group. Table III

TABLE II
DETECTION PERFORMANCE FOR THE STROKE SURVIVORS GROUP IN THE CONTROLLED EXPERIMENT

Subject No	Task Accuracy (%) A (#/60)	B (#/60)	C (#/60)	Overall (#/180) (%)
Subject 1	60 (100%)	59 (98%)	60 (100%)	179 (99.4%)
Subject 2	57 (95%)	60 (100%)	57 (95%)	174 (96.67%)
Subject 3	36 (60%)	50 (83.3%)	58 (96.67%)	144 (80%)
Subject 4	58 (97%)	60 (100%)	60 (100%)	178 (98.9%)
Totals	211/240 (87.92%)	229/240 (95.4%)	235/240 (97.92%)	675/720 (93.75%)

TABLE III
DETECTION PERFORMANCE FOR THE HEALTHY GROUP IN THE CONTROLLED EXPERIMENT

Subject No	Task Accuracy (%) A (#/20)	B (#/20)	C (#/20)	Overall (#/60) (%)
Subject 1	19 (95%)	20 (100%)	20 (100%)	59 (98.3%)
Subject 2	20 (100%)	20 (100%)	18 (90%)	58 (96.67%)
Subject 3	17 (85%)	20 (100%)	20 (100%)	57 (95%)
Subject 4	19 (95%)	19 (95%)	17 (85%)	55 (91.67%)
Subject 5	20 (100%)	19 (95%)	17 (85%)	56 (93.33%)
Subject 6	20 (100%)	20 (100%)	20 (100%)	60 (100%)
Subject 7	20 (100%)	20 (100%)	20 (100%)	60 (100%)
Subject 8	20 (100%)	20 (100%)	20 (100%)	60 (100%)
Subject 9	20 (100%)	19 (95%)	17 (85%)	56 (93.33%)
Subject 10	20 (100%)	20 (100%)	20 (100%)	60 (100%)
Subject 11	20 (100%)	19 (95%)	18 (90%)	57 (95%)
Subject 12	20 (100%)	17 (100%)	20 (100%)	57 (95%)
Subject 13	18 (90%)	19 (95%)	20 (100%)	57 (95%)
Subject 14	18 (90%)	20 (100%)	20 (100%)	58 (96.67%)
Subject 15	20 (100%)	20 (100%)	20 (100%)	60 (100%)
Subject 16	20 (100%)	20 (100%)	20 (100%)	60 (100%)
Subject 17	20 (100%)	20 (100%)	16 (80%)	56 (93.33%)
Subject 18	20 (100%)	20 (100%)	20 (100%)	60 (100%)
Totals	351/360 (97.5%)	352/360 (97.79%)	343/360 (95.28%)	1046/1080 (96.85%)

illustrates the detection performance of the healthy population in the controlled experiment. As anticipated, the level of performance in the healthy group is higher than that of the stroke survivors group. This is attributed to the impaired motor

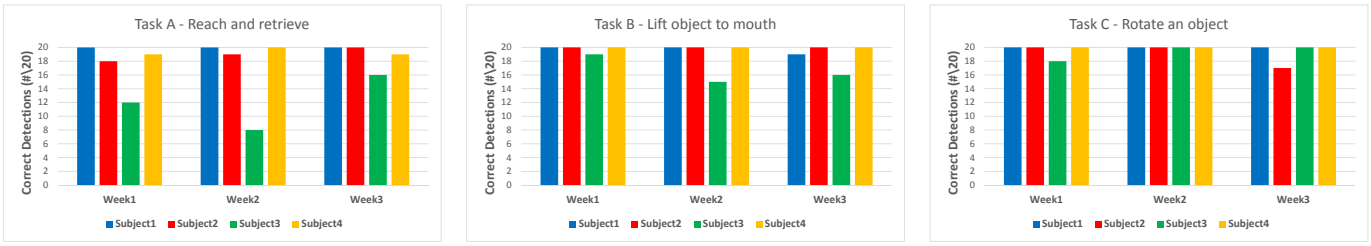

(a) (b) (c)

Fig. 7. The per-week performance of the controlled experiments for (a) Task A (b) Task B and (c) Task C from the stroke survivors group

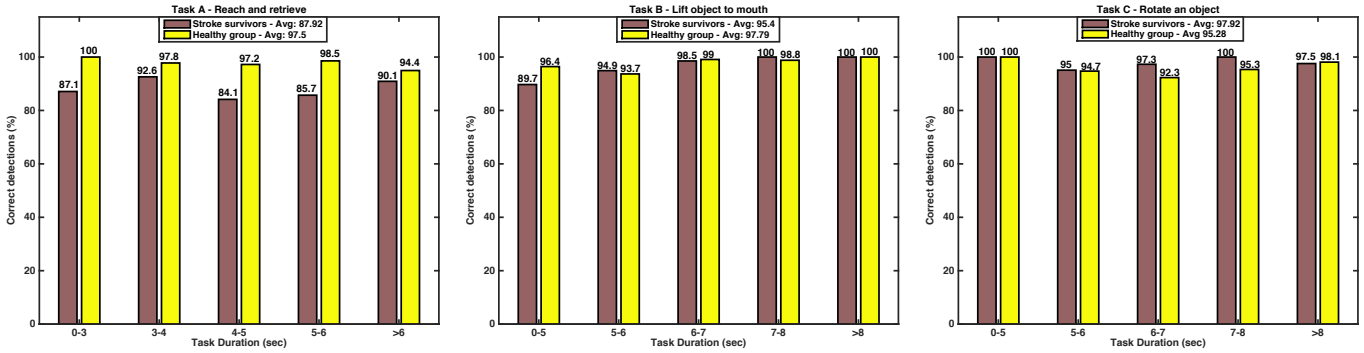

(a) (b) (c)

Fig. 8. Percentage of correct detections against task durations in the controlled experiment for healthy group and stroke survivors. For all tasks the detection ratio remains within $\pm 6\%$ of the average value in both groups (shown in the legend).

function capabilities of the stroke survivors. The combined detection accuracy was higher than 95% for each separate task, when considering all 18 participants. Likewise, a higher than 91% accuracy was obtained for each volunteer, over all tasks. In Table IV the average durations and their respective variances of the tasks performed in the controlled experiment are listed for both groups. To demonstrate the robustness of the detection algorithm against the time a task took to complete, the percentage of correct task detections in the controlled experiment is illustrated in Fig. 8 as a function of task duration for both the stroke survivors and healthy groups. We observe that in both groups and for every task duration, the detection ratio lies within $\pm 6\%$ of the total average detection ratio for this task in the respective group. From this we conclude that the developed algorithm achieves a similar level of performance irrespective of the time required for a task to be completed. Table V and Table VI list the performance results

TABLE IV
AVERAGE TIME DURATIONS OF TASKS IN THE CONTROLLED EXPERIMENT

Task	Duration ($\mu \pm \sigma^2$ sec)	
	Stroke Survivors	Healthy Group
A	4.1±1	5.4±1.3
B	5.9±1.6	6.7±1.7
C	6±2	7.2±1.8

from the semi-naturalistic experiments. The overall detection accuracy remains at high levels ($> 80\%$), although lower than the corresponding figures for the controlled experiment in both groups, as would be expected. Also as expected the accuracy was higher (both overall and for each task) in the healthy group (89%) than in the stroke survivors group (83%). Subject 3 from the stroke survivors group demonstrates the lowest detection accuracies, which we again attribute to their greater level of impairment. Finally, the reason Task A returns a lower level of accuracy, with a close to 80% correct detection ratio, is attributed to the fact that a number of the pre-determined Task A actions in the "preparation of a cup of tea" sequence, such as actions 2,5,12 and 17, are not strictly reach and retrieve actions and were the actions that were misdetected most of the time. During the design of this experiment, however, the expert physiotherapists participating in this study considered these activities as representative of a reach and retrieve action and therefore worthy of inclusion in the experiment.

TABLE V
DETECTION PERFORMANCE FOR THE STROKE SURVIVORS GROUP IN THE SEMI-NATURALISTIC EXPERIMENT

Subject No	Task Accuracy (%)			Overall (#/200) (%)
	A (#/100)	B (#/50)	C (#/50)	
Subject 1	86 (86%)	46 (92%)	44 (88%)	176 (88%)
Subject 2	83 (83%)	45 (90%)	43 (86%)	172 (86%)
Subject 3	61 (61%)	44 (88%)	40 (80%)	145 (72.5%)
Subject 4	88 (88%)	46 (92%)	38 (76%)	172 (86%)
Totals	318/400 (79.5%)	181/200 (90.5%)	165/200 (82.5%)	664/800 (83.00%)

B. Discussion

The experimental investigation achieves two things. Firstly, the high performance in the controlled experiment (93.75% in stroke survivors and 96.85% in the healthy group) among a diverse population, allows us to conclude that the developed

TABLE VI
DETECTION PERFORMANCE FOR THE HEALTHY GROUP IN THE SEMI-NATURALISTIC EXPERIMENT

Subject No	Task Accuracy (%) A (#/40)	B (#/20)	C (#/20)	Overall (#/80) (%)
Subject 1	33 (82.5%)	19 (95%)	20 (100%)	72 (90%)
Subject 2	39 (97.5%)	20 (100%)	20 (100%)	79 (98.75%)
Subject 3	30 (75%)	18 (90%)	20 (100%)	68 (85%)
Subject 4	31 (77.5%)	19 (95%)	18 (90%)	68 (85%)
Totals	133/160 (83.13%)	76/80 (95%)	78/80 (97.5%)	240/260 (89.69%)

algorithm is robust against the variability in the kinematic patterns of different individuals. Additional investigations showed that tasks of different duration are detected with similar high levels of performance in both groups. These observations validate our discrimination strategy and verify that the derived set of rules is capable of discriminating the three movements even in situations where the motor function is impaired. Secondly, with the semi-naturalistic experiment we attempt to evaluate the extent to which the proposed algorithm can detect the three movements when these take place as subtasks of a typical activity (i.e. "preparation of a cup of tea"). The obtained results in this experiment (83% in stroke survivors and 89.69% in the healthy group) are quite promising and indicative of our method's ability to effectively distinguish between the three movements of interest when these take place sequentially. Although the 20 tasks in our experiment were predefined and their sequence was predetermined and not spontaneous, we believe that the semi-naturalistic experiment provides an adequate proof-of-concept. It is common for everyday activities to combine some elements of the three movements. For example the act of drinking a glass of water may involve both a "reach and retrieve" and a "lift object to mouth" action. In such cases, we expect the algorithm to identify the overall activity based on the movement features that characterize it the most.

Analysis of the data shows that incorrect sensor placement can potentially affect the performance of the algorithm. This is because the body coordinate frame of the upper arm and forearm is not perfectly aligned with the two sensor's coordinate frames. When attaching the sensors on the individual's arm we aimed to ensure that the two coordinate frames were closely aligned by visual inspection. More explicit methods for aligning the sensor frame to the body frame like the ones in [31] and [18], were deemed too burdensome and time consuming to be applied to the stroke survivors. In real world use, perfect alignment between the two frames is a very challenging task since body segments are not rigid elements. In addition, in a long-term deployment scenario (like the one we consider), it is not uncommon for attached sensors to move slightly from their original position and thus some degree of misalignment is typically expected to be present. The results show that good performance can be achieved even without perfect alignment which further validates the robustness of the proposed algorithm. In the application scenario we consider, the MARG sensors are expected to be properly placed and aligned to the respective body segment at the beginning of the monitoring session and checked at regular intervals. This can be done by the patients themselves, or if not possible, by a caregiver.

Since the focus of this work was to evaluate the ability of the proposed algorithm to discriminate between the three elementary movements, we decided to manually annotate the obtained datasets, using a marker signal during data acquisition, avoiding any ambiguity in the on/off time instances of the tasks. This annotation strategy, applied both in the controlled and semi-naturalistic experiments, enabled us to isolate the performed tasks in the dataset and exclude from our analysis any other movements performed by the volunteers during the experiments. Naturally, during everyday activities the arm moves around freely and it is not a trivial matter to determine definitively when the start or end of a particular movement or event occurs. This is not as great a problem when the sensors are used during prescribed rehabilitation exercises, since these tend to be directed under supervision. Nevertheless, an automatic event detection system capable of segmenting real time data into periods of activity and inactivity would be necessary for a truly autonomous system (e.g. rehabilitation in the home environment), and this is an area of research that we are currently pursuing. For example, when the arm is not in motion, the modulus of the combined tri-axial accelerometer signal equates to the value of gravitational acceleration, whilst the modulus of the combined tri-axial gyroscope signal equates to zero and similarly the modulus of the combined tri-axial magnetometer signal equates to the local value of magnetic field strength, irrespective of sensor orientation. Although the last of these factors is also dependant on geographical location and magnetometers can be influenced by the proximity of ferrous materials [32] which are likely to be present in the home environment, it is possible by employing a simple thresholding technique on these sensor signals to distinguish periods of activity from inactivity; a crude form of event detection. It is established that density estimation algorithms (e.g. Kalman Filters, Particle Filters) coupled with more complex modeling of the arm, based on physical geometrical constraints, can provide a more accurate estimation of the upper limb orientation, minimizing the effect of gyroscope drift [18], [31]. Typically, the natural restriction of the human elbow in performing abduction/adduction is used to correct an initial orientation estimation in such a way that the elbow abduction/adduction angle is minimized. However, the computational load in such approaches is considerably high, thus we employed the more efficient quaternion gradient descent method. Here, the gyroscope drift is compensated using the parameter β, that represents the gyroscope measurement error as the magnitude of a quaternion derivative [12]. To demonstrate the ability of the orientation algorithm to mitigate the gyroscope error, we calculate the elbow abduction/adduction angle, as the angle between the Z-axis of the forearm and the Y-axis of the upper arm minus $90\,\mathrm{deg}$, for the three movements executed by healthy volunteers in the controlled experiment. From Fig. 9, we observe that the angle remains small (almost always $< 10^{\circ}$) in all three movements. From this we conclude that, although less accurate than the Particle Filter approach in [31], the quaternion gradient descent method provides a

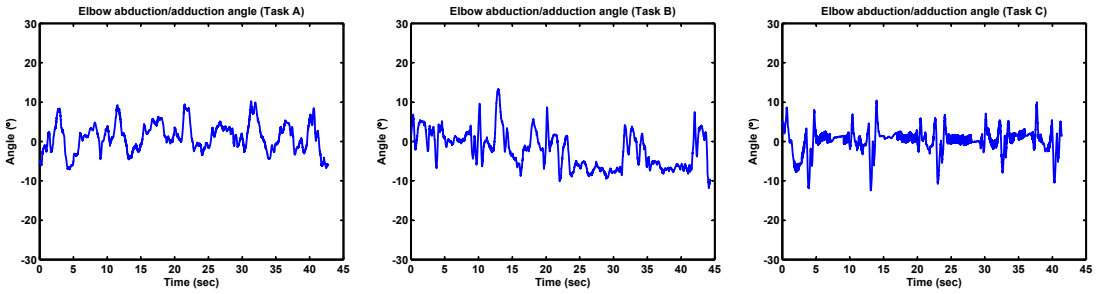

(a) (b) (c)

Fig. 9. The elbow abduction/adduction angle calculated in the three tasks, (a) Task A (b) Task B and (c) Task C.

reasonably accurate estimation of the orientation of the upper limb.

VI. Conclusions

This paper describes the development of an algorithmic solution for efficiently detecting and discriminating three elementary arm movements. These movements are fundamental in natural activities and the ability to detect them is of great importance in evaluating the rehabilitation progress of stroke survivors or patients suffering from other motor neuron diseases. In our work, we employ a pair of MARG sensors attached to the wrist and elbow, from which the orientation of the arm segments are deduced using a gradient-descent quaternion based method. With the aid of a 2-link limb model and position vectors, 3-D tracking of the upper arm and forearm position is achieved. From the kinematic analysis a set of rules, involving three kinematic parameters (e_fe, s_fe and v_f^z), was derived and used to formulate the detection and discrimination algorithm. The proposed solution was then evaluated in a series of experiments with two groups, healthy individuals (18 subjects) and stroke survivors (4 subjects). In the controlled experiments the proposed algorithm achieved $>88\%$ performance for each task individually and $>93\%$ overall across both groups. This validates the basic rules of our detection algorithm and establishes its robustness. This is further solidified by the ability to identify tasks of different duration with similar accuracy, ($\pm 6\%$ of the average value) in both groups. Similar levels of performance, $>80\%$ for each separate task and $>83\%$ overall, were also obtained in the semi-naturalistic experiments which, although predefined, comprise a sequence of the three tasks that represent a typical everyday activity: "preparing a cup of tea". This level of accuracy demonstrates the potential of the proposed method in identifying the three elementary upper limb movements during natural activities. Combined with the computationally inexpensive orientation algorithm, the work discussed in this paper has clear potential of being integrated in a body-area-network of MARG sensors as a component of a fully automated task detection and discrimination system for home-based rehabilitation applications.

References

[1] A. S. Go, D. Mozaffarian, V. L. Roger, E. J. Benjamin, J. D. Berry, M. J. Blaha, S. Dai, E. S. Ford, C. S. Fox, S. Franco, H. J. Fullerton, C. Gillespie, S. M. Hailpern, J. A. Heit, V. J. Howard, M. D. Huffman, S. E. Judd, B. M. Kissela, S. J. Kittner, D. T. Lackland, J. H. Lichtman, L. D. Lisabeth, R. H. Mackey, D. J. Magid, G. M. Marcus, A. Marelli, D. B. Matchar, D. K. McGuire, E. R. Mohler, C. S. Moy, M. E. Mussolino, R. W. Neumar, G. Nichol, D. K. Pandey, N. P. Paynter, M. J. Reeves, P. D. Sorlie, J. Stein, A. Towfighi, T. N. Turan, S. S. Virani, N. D. Wong, D. Woo, and M. B. Turner, "Heart disease and stroke statistics2014 update: A report from the american heart association," *Circulation*, vol. 129, no. 3, pp. e28–e292, Jan 2014.

[2] V. L. Feigin, M. H. Forouzanfar, R. Krishnamurthi, G. A. Mensah, M. Connor, D. A. Bennett, A. E. Moran, R. L. Sacco, L. Anderson, T. Truelsen, M. O'Donnell, N. Venketasubramanian, S. Barker-Collo, C. M. M. Lawes, W. Wang, Y. Shinohara, E. Witt, M. Ezzati, M. Naghavi, and C. Murray, "Global and regional burden of stroke during 1990-2010: findings from the global burden of disease study 2010," *Lancet*, vol. 383, no. 9913, pp. 245 – 255, Jan 2014.

[3] I. Korhonen, J. Parkka, and M. Van Gils, "Health monitoring in the home of the future," *IEEE Eng. Med. Biol.*, vol. 22, no. 3, pp. 66–73, May 2003.

[4] P. Bonato, "Wearable sensors and systems," *IEEE Eng. Med. Biol.*, vol. 29, no. 3, pp. 25–36, May 2010.

[5] StrokeBack Project, Sep 2014. [Online]. Available: www.strokeback.eu

[6] S. L. Wolf, P. A. Catlin, M. Ellis, A. L. Archer, B. Morgan, and A. Piacentino, "Assessing wolf motor function test as outcome measure for research in patients after stroke," *Stroke*, vol. 32, no. 7, pp. 1635–1644, Jul 2001.

[7] S. L. Fritz, S. Blanton, G. Uswatte, E. Taub, and S. L. Wolf, "Minimal detectable change scores for the wolf motor function test," *Neurorehabil Neural Re.*, vol. 23, no. 7, pp. 662–669, Sep 2009.

[8] B. Najafi, K. Aminian, A. Paraschiv-Ionescu, F. Loew, C. Bula, and P. Robert, "Ambulatory system for human motion analysis using a kinematic sensor: monitoring of daily physical activity in the elderly," *IEEE Trans. Biomed. Eng.*, vol. 50, no. 6, pp. 711–723, Jun 2003.

[9] A. Salarian, H. Russmann, F. Vingerhoets, P. Burkhard, and K. Aminian, "Ambulatory monitoring of physical activities in patients with parkinson's disease," *IEEE Trans. Biomed. Eng.*, vol. 54, no. 12, pp. 2296–2299, Dec 2007.

[10] P. Veltink, H. Bussmann, W. de Vries, W. L. Martens, and R. van Lummel, "Detection of static and dynamic activities using uniaxial accelerometers," *IEEE Trans. Rehabil. En.*, vol. 4, no. 4, pp. 375–385, Dec 1996.

[11] L. Wang, T. Gu, X. Tao, and J. Lu, "A hierarchical approach to real-time activity recognition in body sensor networks," *Pervasive and Mobile Computing*, vol. 8, no. 1, pp. 115 – 130, Feb 2012.

[12] S. Madgwick, A. J. L. Harrison, and R. Vaidyanathan, "Estimation of imu and marg orientation using a gradient descent algorithm," in *2011 IEEE Int. Conf. on Rehabilitation Robotics*, Jun 2011, pp. 1–7.

[13] D. Biswas, A. Cranny, N. Gupta, K. Maharatna, J. Achner, J. Klemke, M. Jöbges, and S. Ortmann, "Recognizing upper limb movements with wrist worn inertial sensors using k-means clustering classification," *(accepted, in press) Hum. Mov. Sci.*, vol. 40, pp. 59–76, Apr 2015.

[14] R. Hyde, L. Ketteringham, S. Neild, and R. Jones, "Estimation of upper-limb orientation based on accelerometer and gyroscope measurements," *IEEE Trans. Biomed. Eng.*, vol. 55, no. 2, pp. 746–754, Feb 2008.

[15] M. El-Gohary and J. McNames, "Shoulder and elbow joint angle tracking with inertial sensors," *IEEE Trans. Biomed. Eng.*, vol. 59, no. 9, pp. 2635–2641, Sep 2012.

[16] D. Roetenberg, P. Slycke, and P. Veltink, "Ambulatory position and

orientation tracking fusing magnetic and inertial sensing," *IEEE Trans. Biomed. Eng.*, vol. 54, no. 5, pp. 883–890, May 2007.

[17] H. Zhou, H. Hu, N. D. Harris, and J. Hammerton, "Applications of wearable inertial sensors in estimation of upper limb movements," *Biomed. Signal Process. Control*, vol. 1, no. 1, pp. 22 – 32, Jan 2006.

[18] H. Luinge, P. Veltink, and C. Baten, "Ambulatory measurement of arm orientation," *J. Biomech.*, vol. 40, no. 1, pp. 78–85, 2007.

[19] X. Yun and E. Bachmann, "Design, implementation, and experimental results of a quaternion-based kalman filter for human body motion tracking," *IEEE Trans. Robot.*, vol. 22, no. 6, pp. 1216–1227, Dec 2006.

[20] R. Mahony, T. Hamel, and J.-M. Pflimlin, "Nonlinear complementary filters on the special orthogonal group," *IEEE Trans Autom. Control*, vol. 53, no. 5, pp. 1203–1218, Jun 2008.

[21] N. Keijsers, M. Horstink, and S. Gielen, "Online monitoring of dyskinesia in patients with parkinson's disease," *IEEE Eng. Med. Biol.*, vol. 22, no. 3, pp. 96–103, May 2003.

[22] L. Atallah, B. Lo, R. King, and G.-Z. Yang, "Sensor positioning for activity recognition using wearable accelerometers," *IEEE Trans. Biomed. Circuits Syst.*, vol. 5, no. 4, pp. 320–329, Aug 2011.

[23] O. Banos, M. Damas, H. Pomares, A. Prieto, and I. Rojas, "Daily living activity recognition based on statistical feature quality group selection," *Expert Syst Appl*, vol. 39, no. 9, pp. 8013 – 8021, Jul 2012.

[24] D. Rodríguez-Martín, C. Pérez-López, A. Samà, J. Cabestany, and A. Català, "A wearable inertial measurement unit for long-term monitoring in the dependency care area," *Sensors*, vol. 13, no. 10, pp. 14 079–14 104, Oct 2013.

[25] M. Ermes, J. Parkka, J. Mantyjarvi, and I. Korhonen, "Detection of daily activities and sports with wearable sensors in controlled and uncontrolled conditions," *IEEE Trans. Inf. Technol. Biomed.*, vol. 12, no. 1, pp. 20–26, Jan 2008.

[26] J. Parkka, M. Ermes, P. Korpipaa, J. Mantyjarvi, J. Peltola, and I. Korhonen, "Activity classification using realistic data from wearable sensors," *IEEE Trans. Inf. Technol. Biomed.*, vol. 10, no. 1, pp. 119–128, Jan 2006.

[27] A. Fleury, M. Vacher, and N. Noury, "Svm-based multimodal classification of activities of daily living in health smart homes: Sensors, algorithms, and first experimental results," *IEEE Trans. Inf. Technol. Biomed.*, vol. 14, no. 2, pp. 274–283, Mar 2010.

[28] S. Patel, K. Lorincz, R. Hughes, N. Huggins, J. Growdon, D. Standaert, M. Akay, J. Dy, M. Welsh, and P. Bonato, "Monitoring Motor Fluctuations in Patients With Parkinson's Disease Using Wearable Sensors," *IEEE Trans. Inf. Technol. Biomed.*, vol. 13, no. 6, pp. 864–873, Nov 2009.

[29] H. Junker, O. Amft, P. Lukowicz, and G. Tr "Gesture spotting with body-worn inertial sensors to detect user activities," *Pattern Recogn.*, vol. 41, no. 6, pp. 2010 – 2024, Jun 2008.

[30] A. Burns, B. Greene, M. McGrath, T. O'Shea, B. Kuris, S. Ayer, F. Stroiescu, and V. Cionca, "Shimmer^{TM} - a wireless sensor platform for noninvasive biomedical research," *IEEE Sensors J.*, vol. 10, no. 9, pp. 1527–1534, Sep 2010.

[31] Z.-Q. Zhang and J.-K. Wu, "A novel hierarchical information fusion method for three-dimensional upper limb motion estimation," *IEEE Trans. Instrum. Meas.*, vol. 60, no. 11, pp. 3709–3719, Nov 2011.

[32] C. Kendell and E. D. Lemaire, "Effect of mobility devices on orientation sensors that contain magnetometers," *J. Rehab. Res. Dev.*, vol. 46, no. 7, pp. 957–962, 2009.